

Sigmoidal particle density distribution in a subplinian scoria fall deposit

Julia Eychenne · Jean-Luc Le Pennec

Received: 3 April 2012 / Accepted: 28 September 2012 / Published online: 10 October 2012
© Springer-Verlag Berlin Heidelberg 2012

Abstract A general expression to describe particle density distribution in tephra fall deposits is essential to improve fallout tephra mass determination and numerical modelling of tephra dispersion. To obtain particle density distributions in tephra fall deposits, we performed high-resolution componentry and particle density analyses on samples from the 2006 subplinian eruption of Tungurahua volcano in Ecuador. Six componentry classes, including pumice and scoria, have been identified in our sample collection. We determined the class of 300 clasts in each 0.5 ϕ fractions from -4.5ϕ to 3.5ϕ and carried out water pycnometry density measurements on selected size fractions. Results indicate that the mean particle density increases with ϕ up to a plateau of $\sim 2.6 \text{ g/cm}^3$ for clasts finer than 1.5ϕ . The density of scoria and pumice increases between -3 and 1ϕ , while dense particle density is sub-constant with grainsize. We show that the mean particle density μ of the vesicular fractions is a function of grainsize i (ϕ scale) given by a sigmoidal law: $\mu(i) = K + \beta/(1 + \alpha e^{-ri})$, where K , β , α and r are constants. These sigmoidal distributions can be used to determine accurately the load of each componentry class and should be applicable to many tephra deposits and for modelling purposes.

Keywords Density distributions · Sigmoidal law · Componentry proportions · Volume-to-mass conversion

Introduction

Characterizing the size of explosive eruptions is important for hazard studies and requires determining magnitude and intensity in terms of volume or mass. This can be achieved from analyses of tephra deposits and numerical modelling approaches, which require documenting grainsize and particle density distributions, and tephra dispersal pattern (Pyle 2000; Costa et al. 2006; Barsotti and Neri 2008). Notably, a general formulation for particle density distribution in tephra fall deposit is essential to convert particle volume fractions—e.g. from componentry analyses—to mass proportions (e.g. Taddeucci et al. 2002; Andronico et al. 2009; Araña-Salinas et al. 2010), enabling improved eruption size determinations. In addition, particle density distributions, which depend on grain size and vesicularity, control terminal settling velocity and depositional patterns, and a thorough documentation of these is required to improve current numerical models (e.g. Bonadonna and Phillips 2003; Costa et al. 2006; Barsotti and Neri 2008). However, a general expression of particle density distribution in tephra fall deposits is still lacking. Previous attempts considered simple distributions with constant density values in a range of grainsize (e.g. Taddeucci et al. 2002; Costa et al. 2006; Folch et al. 2008; Andronico et al. 2009; Araña-Salinas et al. 2010) and a linear density variation between extreme plateau values for coarse (-4 to -1ϕ) and fine ($>7\phi$) grainsize end-members (Bonadonna and Phillips 2003; Alfano et al. 2011), a representation that has not been confirmed from extended analyses of volcanic deposits. Based on high-resolution componentry and density analyses of a subplinian scoria fall layer from the August 16, 2006 eruption of Tungurahua volcano, Ecuador, we show here that

Editorial responsibility: V. Manville

J. Eychenne (✉) · J.-L. Le Pennec
OPGC, Laboratoire Magmas et Volcans, Clermont Université,
Université Blaise Pascal,
BP 10448, 63000 Clermont-Ferrand, France
e-mail: j.eychenne@opgc.univ-bpclermont.fr

J. Eychenne · J.-L. Le Pennec
CNRS, UMR 6524, LMV,
63038 Clermont-Ferrand, France

J. Eychenne · J.-L. Le Pennec
IRD, R 163, LMV,
63038 Clermont-Ferrand, France

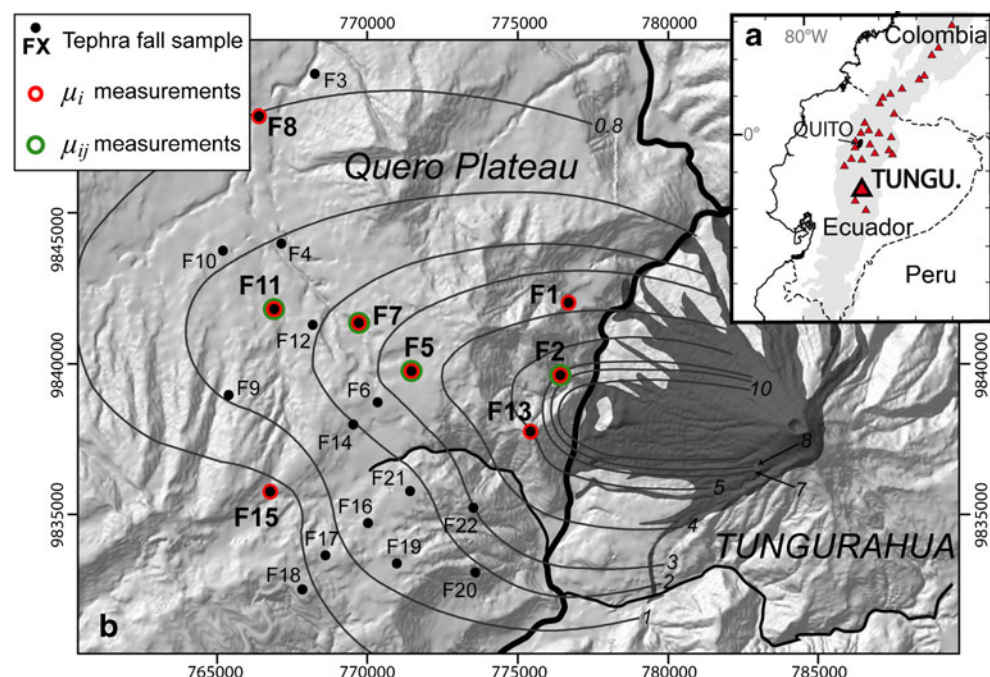
density distributions of different componentry classes can be precisely described by a sigmoidal law. We infer that it can be used for eruption size evaluation and modelling of tephra dispersal and sedimentation patterns.

Tungurahua is a 5,023 m-high andesitic stratovolcano located in the Eastern Andean Cordillera of Ecuador (Fig. 1a). It is frequently active and reawakened in 1999 after 80 years of dormancy (Le Pennec et al. 2012). Since then, ongoing activity has comprised phases of uneven intensity, size (VEI 1 to VEI 3) and style (strombolian, vulcanian, subplinian). The paroxysmal phase occurred on August 16–17, 2006 and lasted for about 6 hours: a tephra column rose more than 15 km above the crater and the plume deposited a dark scoria and ash fall layer to the west in the InterAndean highlands, while numerous pyroclastic scoria flows descended the flanks of the volcano (Kelfoun et al. 2009) (Fig. 1b). This eruption produced a bulk tephra volume in the range of $47\text{--}67 \times 10^6 \text{ m}^3$ and ranked as VEI 3 (Eychenne et al. 2012).

Methodology

The deposit was sampled at 22 sites (Fig. 1b) on flat surfaces of known area a (all symbols used here and below are reported in Table 1). The samples were dried in the laboratory, weighed and sieved at a 0.5ϕ interval ($= -\log_2 \delta$, δ being the particle diameter in mm) in the range $-4.5\text{--}4\phi$ (22.4 mm–63 μm) (Eychenne et al. 2012). The mass m_i of each grainsize fraction i was measured on a high-precision balance (10^{-2} g).

Fig. 1 **a** Location map of Tungurahua volcano in the Andean Cordillera of Ecuador. **b** Shaded relief map of Tungurahua edifice and the area of tephra fall (on the Quero Plateau) and pyroclastic flow (dark grey area) deposits. Isopachs are in centimeters (grey curves, from Eychenne et al. (2012)). Small dots are sampling sites for grainsize studies ($F1\text{--}F22$ are sample numbers), and large open circles identify sites of samples analysed in this study



Componentry analyses

Based on textural criteria (shape, colour, vesicularity), six pyroclast classes have been distinguished in our sample collection. (1) The Scoria class (S): ragged, dark to brown juvenile vesicular particles with homogeneous andesitic composition (57.6–58.9 wt.% SiO₂; Samaniego et al. 2011). (2) The Pumice class (P): light-toned, highly vesicular juvenile clasts with a more siliceous composition (61.1–62.5 wt.% SiO₂; Samaniego et al. 2011), showing a glassy texture and sub-spherical vesicle shapes. (3) The Free Crystal class (C): mainly euhedral plagioclase and pyroxene, with irregular glass coating. (4) The Dense Lithic class (D): dark blocky, micro-crystalline non-vesicular clasts. (5) The Crystalline Aggregate class (A): assemblages of plagioclase and pyroxene crystals with little or no interstitial glass. (6) The Reddish Scoria class (R): sub-rounded, moderately vesicular grains with cavities and vesicles, about 100–50 μm in diameter, showing weathering and vapour-phase minerals on their surface.

We determined the volume proportions of the componentry classes by particle identification and counting in each grainsize fraction from -4.5ϕ to 3.5ϕ . The fraction was distributed as a circle on a flat surface, and carefully homogenized by mixing up the grains with a thin spatula from the edge to the centre. We then isolated half of the material in a half-circle to begin particle determination and counting from its centre to its edge. The analyses were carried out by the naked eye below 0.5ϕ and under a binocular microscope at higher ϕ . Above -1ϕ , the counting operation was performed independently two to

Table 1 Summary of the notations used in this study

Symbol	Definition (unit)
a	Sampling area (m^2)
α	Constant parameter of the sigmoidal function
β	Constant parameter of the sigmoidal function
c_{ij}	Percentage of particles of the componentry class j in the grainsize fraction i
δ	Particle diameter (mm)
ϕ	Unit for grainsize calculated as $\phi = -\log_2 \delta$
i	Grainsize in a half- ϕ scale
j	Componentry class (from S (Scoria class) to R (Reddish Scoria class))
K	Constant parameter of the sigmoidal function
$m_{A_{ij}}$	Mass per unit area of particles from the componentry class j in the grainsize fraction i (g/m^2)
m_i	Mass of particles in the grainsize fraction i (g)
m_{ij}	Mass of particles in the componentry class j of the grainsize fraction i (g)
μ_i	Mean particle density in the grainsize fraction i (g/cm^3)
$\mu(i)$	Continuous function describing the variations of the particle density with ϕ in the samples
μ_{ij}	Mean particle density in the componentry class j of the grainsize fraction i (g/cm^3)
particle%	Percentage of particles
r	Constant parameter of the sigmoidal function
v_i	Total particle volume in the grainsize fraction i (cm^3)
v_{ij}	Volume of particles in the componentry class j of the grainsize fraction i (cm^3)

four times by two operators, depending on the stability and reproducibility of the results. Results in a single grainsize fraction i are expressed as c_{ij} , the percentage of particles (particle %) in each componentry class j (j from S to R) of the grainsize fraction i . For a given grainsize fraction we calculated the mean and the standard deviation of all the componentry results in particle % obtained after the counting operations. Counting results out of the interval defined by “mean \pm standard deviation” were discarded for a standard deviation higher than 2. Repeated counting on test-samples indicated that 250 ± 20 particle determinations are required to obtain stable componentry proportions, i.e. varying in an interval of 3 % of particle proportions. Thus, we counted at least 300 grains, or the whole grainsize fraction population when it contained less than 300 grains.

Particle density measurements

Water pycnometry was used to measure μ_i , the mean particle density in the grainsize fraction i , and μ_{ij} , the mean particle density in the componentry class j of the grainsize fraction i , given respectively by:

$$\mu_i = m_i/v_i \quad (1)$$

$$\mu_{ij} = m_{ij}/v_{ij} \quad (2)$$

where v_i is the total particle volume in the grainsize fraction i , and v_{ij} and m_{ij} are the volume and the mass of particles in the componentry class j in the grainsize fraction i ,

respectively. The measurements were performed on a high-precision balance (10^{-3} g) with 0.1 and 0.5 dm³ boro-silicate pycnometers, using distilled and degassed water. The water was observed to wrap the particles—previously dried—without filling the pores in the studied grainsize range (-2.5 – 3ϕ), due to relatively high water surface tension and small bubble size in the particles. Weighing was performed rapidly after particle incorporation (<3 min) and we thus assume negligible water incorporation in the clasts during pycnometry analyses. The soundness of this assumption is supported by the variation trend of the resulting data (see “Particle densities” section) and the reproducibility of the measurements (see below).

The mean particle density in the grainsize fraction i , μ_i , was measured using 1 to 4 g of particles in selected grainsize fractions from eight tephra samples collected along the main dispersal axis (“near-to-axis”) and laterally on the margins of the deposit (“off-axis”) (Fig. 1b). μ_i measurements were performed three times in each grainsize fraction of sample F7 to evaluate the reproducibility of pycnometry analyses. The standard deviation of the results of these measurements is between 0.02 and 0.04.

The mean particle density of the componentry class j in the grainsize fraction i , μ_{ij} , was determined for pumice (μ_{iP}), scoria (μ_{iS}) and dense lithic (μ_{iD}) classes using several particles (from 10 to 100) of each componentry class isolated from selected grainsize fractions in the range -2.5 – 1ϕ , in four near-to-axis tephra samples (Fig. 1b). μ_{ij} was not measured in grainsize fractions finer than 1ϕ due to the difficulty in separating the different types of clasts. For grainsize

fractions with too few particles in a single componentry class (e.g. pumices and dense lithics), we merged several fractions to obtain a mass of grains large enough to ensure reliable pycnometry weighing.

Results

Size-dependent componentry proportions

The results are represented as the numerical proportions of the 6 componentry classes in particle % vs. grainsize (Fig. 2a) for three near-to-axis samples (F5, F7 and F11, Fig. 1b). They all show similar proportion variations: (1) S and C are dominant classes; (2) S proportions are >90 particle % in fractions coarser than -1.5ϕ and decrease with ϕ , reaching a minimum between 0 and 1ϕ , and increasing again in fine fractions up to $\sim 2.5\phi$; (3) C occurs in fractions finer than -2ϕ and displays a negative correlation to S; (4) in the studied size range the A proportion is <5 particle %, peaking between 0 and 1ϕ ; (5) R occurs above 0ϕ and increases regularly with ϕ ; (6) P is sub-constant around 1 particle %; (7) D is concentrated in the coarse size range ($<-2.5\phi$) for proximal samples (F5 and F7) and shows stable proportions <2 particle % in finer grainsizes.

Fig. 2 **a** Plots of componentry analyses of three near-to-axis samples (see Fig. 1) in percentages of particles. Symbol size is larger than the error bar defined as \pm the standard deviation (1σ). **b** Componentry mass per unit area, mA, (in mg/cm^2) vs. grainsize, after converting the componentry proportions in particle %. *F*-labels are sample numbers (see Fig. 1 for location)

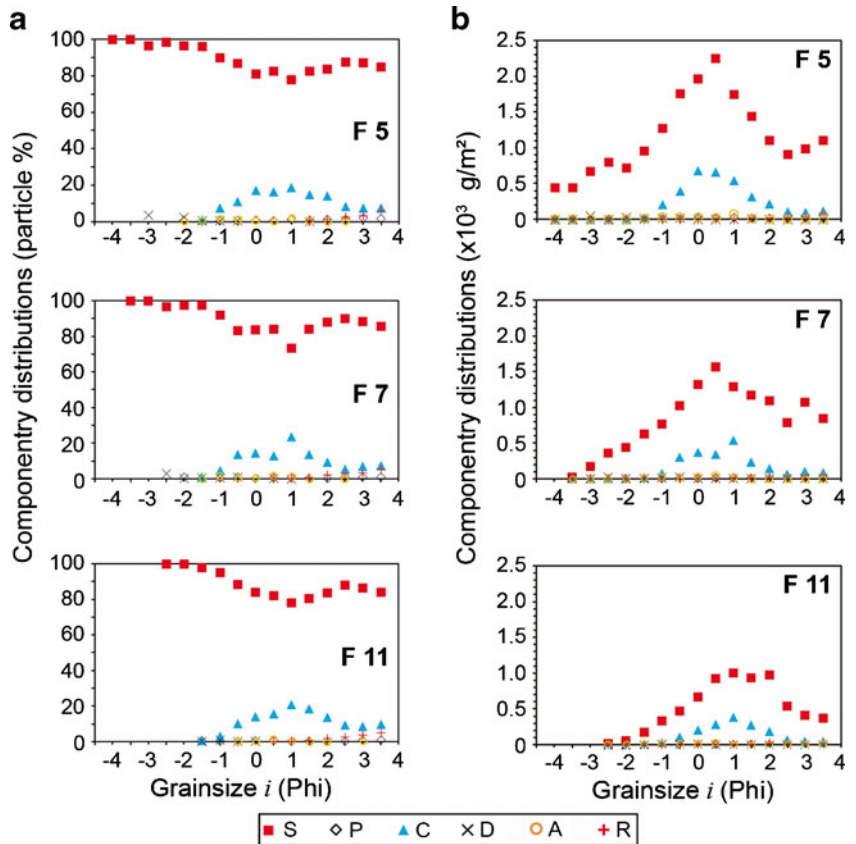
Particle densities

In our sample collection, the mean particle density, μ_i , varies with grainsize i following similar trends (Fig. 3a): μ_i increases with ϕ , and stabilizes near a maximum constant value above 1.5ϕ . While the samples show, in the coarse size range, a wide range of μ_i values (for instance $\mu_{-1\phi}$ is between 1.04 and $1.88 \text{ g}/\text{cm}^3$), the density range narrows with increasing ϕ , and μ_i converges to a sub-constant value close to $\sim 2.6 \text{ g}/\text{cm}^3$. In near-to-axis samples, μ_i decreases with distance from the vent in coarse grainsizes (-1 , 0 and 1ϕ) and is constant in 2 and 3ϕ fractions (Fig. 3b). The densities measured in the classes P, S and D show (Fig. 3c): (1) μ_{iD} values are in the range $2.61\text{--}2.73 \text{ g}/\text{cm}^3$ and show no correlation to grainsize; (2) μ_{iS} increases with ϕ ; and (3) for each grainsize fraction $\mu_{iP} < \mu_{iS}$ by at least $0.20 \text{ g}/\text{cm}^3$.

Size-dependent particle density distributions

In all samples, the variation of the density μ_i vs. grainsize i is fitted well by a sigmoidal function of the form:

$$\mu(i) = K + \beta / (1 + \alpha e^{-ri}) \quad (3)$$



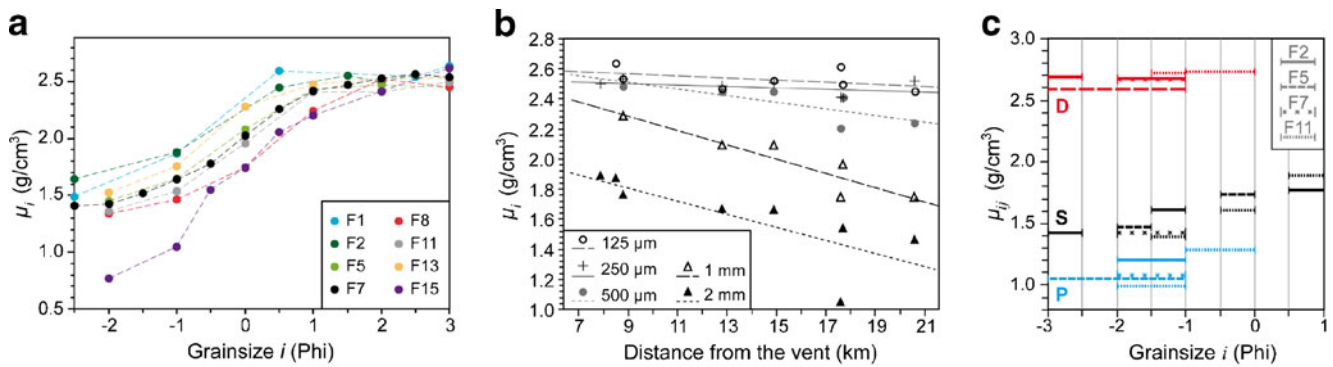


Fig. 3 a and b Plots of mean particle densities in the grainsize fractions μ_i (in g/cm³) obtained using water pycnometry analyses vs. grainsize and distance from vent. Symbol size is larger than the error bar defined as \pm the standard deviation (1σ ; evaluated from the results of three sets of measurements performed on sample F7). c Plots of the

particle density in the componentry classes μ_{ij} (in g/cm³) vs. grainsize, obtained by water pycnometry analyses in selected grainsize fractions or merged grainsize fractions. D Dense Lithics; S Scoriae; P Pumices. F-labels are sample numbers (see Fig. 1 for location)

where K , β , α and r are constants (Fig. 4). Pycnometry analyses show that μ_{iD} results are sub-constant with grainsize (Fig. 3c). Because of physical and chemical grain homogeneity in D, R, C and A classes, we set μ_{iD} , μ_{iR} , μ_{iC} and μ_{iA} as constant within the grainsize range and independent of sampling location.

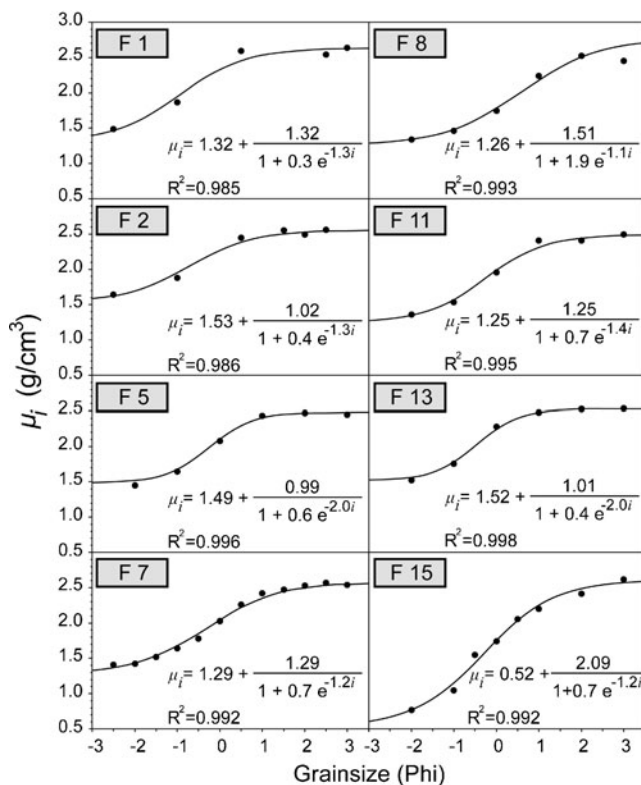


Fig. 4 Sigmoidal fit (solid curve) of μ_i data points (the mean particle densities in the grainsize fractions measured by pycnometry; black dots) for the height tephra samples analysed in this study. Equations of the best sigmoidal fit for each sample are reported on the plots. F-labels are sample numbers (see Fig. 1 for location)

μ_{iD} is calculated as the mean of the pycnometry results (2.68 g/cm³, Fig. 3c), and μ_{iR} , μ_{iC} and μ_{iA} values are set to 2.60, 2.90 and 2.90 g/cm³, respectively, based on petrological constraints (Samaniego et al. 2011) and additional data from the literature (Clark 1966).

As S is by far the dominant clast population in the deposit (Fig. 2a), the sigmoidal pattern of μ_i vs. grainsize i (Fig. 3a and 4) is mainly controlled by μ_{iS} . Results of S density measurements show that μ_{iS} increases with grainsize i in the range $-2.5-1\phi$ (Fig. 3c). No data were obtained in the fine fraction beyond 1.5ϕ , we thus assume a constant variation of μ_{iS} in grainsize fractions $\geq 2\phi$, based on the variations of the mean particle density μ_i . We set the plateau density value to that of a pore-free andesitic glass (2.47 g/cm³; Clark 1966) and calculated a sigmoidal fit to a dataset that includes the measured densities and the plateau value beyond 1.5ϕ . As vesicle textures of P and S are similar, we surmise that the variation of P density vs. grainsize also follows a sigmoidal trend. As glass composition in P is rhyolitic (Samaniego et al. 2011), we can use the same interpolation method with a plateau density value close to that of a pore-free rhyolitic glass (2.37 g/cm³; Clark 1966). The reconstructed mean particle density in the grainsize fraction (μ_i') is calculated from μ_{ij} , assuming that in a given grainsize fraction the particles have similar size and using the following equation:

$$\mu_i = \sum_j c_{ij} \mu_{ij} \quad (4)$$

where c_{ij} is the proportion of the componentry class j in the grainsize fraction i in particle %. The results are in good agreement with the sigmoidal fit of the density measurements ($\mu(i)$) (Fig. 5).

Volume-to-mass conversion of componentry distributions

Here, we use the sigmoidal law to convert componentry results from particle % to mA , the mass per unit area. Considering that all particles at each sampling site in a given size fraction have the same size, the proportion of the componentry class j in the grainsize fraction i in particle % (c_{ij} , Fig. 2a) can be converted to mass per unit area of the componentry class j in the grainsize fractions i (mA_{ij}) using the equation:

$$mA_{ij} = (\mu_{ij} c_{ij} m_i) / (\mu_i a) \quad (5)$$

where m_i is the mass of each grainsize fraction i and a is the sampling area. Thus, continuous expressions of particle density distributions (for the grainsize fractions and the componentry classes) are required for mass conversion over the full grainsize range. We use the sigmoidal approach inferred above for μ_i and μ_{ij} to convert the componentry results for three near-to-axis samples (F5, F7 and F11, Fig. 1b). Figure 2b illustrates the three resulting componentry distributions in terms of mass per unit area. Among the classes mA_{iS} shows the highest values (maxima between 2.25×10^3 and 1.00×10^3 g/m²), which decrease away from vent. mA_{iC} varies in a narrow grainsize range (-1ϕ – 2ϕ) along a bell-

shaped trend whose amplitude decreases distally. The mass per unit area of other componentry classes are small and sub-constant, on the order of 1 to 600 g/m².

Discussion

Origin of the sigmoidal density distribution

The sigmoidal pattern evidenced for μ_{iS} and μ_{iP} vs. grainsize i is interpreted here as a consequence of size-dependant vesicularity distributions in the clast populations: pore-free particles (e.g. glass shards and bubble walls) tend to be the dominant material when clast size is smaller than that of vesicles, as documented in basaltic ash and silicic pumice particles (e.g. Heiken and Wohletz 1985; Manville et al. 2002). The plateau values reached by μ_{iS} and μ_{iP} in the fine size range above 1.5 – 2ϕ , at ~ 2.5 and ~ 2.4 g/cm³, respectively, represent the solid density of scoria and pumice grains, which is close to the density of the groundmass silicate glass. The mean particle density variations (μ_i) reflect the sigmoidal distribution of the dominant S class. The μ_i plateau value (~ 2.6 g/cm³) is an averaged solid density for all grains of the deposit and is higher than the scoria's solid density, implying that average densities are higher for the other componentry classes.

Implication of the sigmoidal density distribution pattern

Particle density data are essential to calculate particle settling velocities and are thus required in numerical tephra dispersion models. Most current models use two or three particle density values increasing with ϕ (Costa et al. 2006; Scollo et al. 2007; Folch et al. 2008). Based on literature surveys, Bonadonna and Phillips (2003) have proposed particle density models based on different chemical magma compositions, which assume constant pumice density from -4ϕ to -1ϕ , a linear increase with ϕ , and a plateau value equal to a lithic density for grainsizes $>7\phi$. This study indicates that the grainsize-density relationship, at least in the 2006 Tungurahua scoria fall layer, is more accurately described by a sigmoidal law, and the plateau value in the least dense fine tail end-member is reached for coarser particles, around 2ϕ .

Further studies on well-preserved tephra fall deposits are required to assess whether the sigmoidal expression evidenced here for the August 2006 Tungurahua tephra layer is generally applicable. Suggesting that it may be, the August 2006 Tungurahua deposit is an archetypal subplinian scoria fall layer with componentry content and vesicularity distribution patterns of juvenile clasts similar to that of violent strombolian eruptions (e.g. Arrighi et al. 2001; Pioli et al. 2008). We thus surmise that the density distribution pattern evidenced at Tungurahua is most likely applicable to many other tephra fall deposits. This sigmoidal law can be easily parameterized

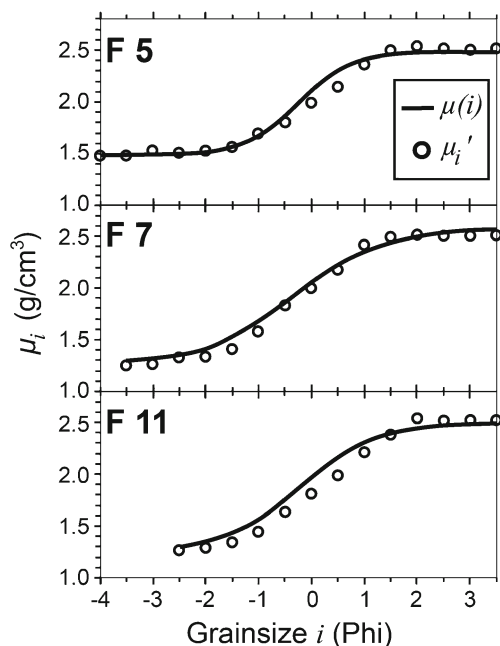


Fig. 5 Plots of $\mu(i)$, the mean particle density function in the grainsize fractions determined by sigmoidal interpolation of water pycnometry data, and μ'_i , the mean particle densities in grainsize fractions reconstructed using a linear combination of the componentry densities vs. grainsize i (ϕ). μ_i and μ'_i in g/cm³. F-labels are sample numbers (see Fig. 1 for location)

using a few density measurements in different grainsize fractions, given that the critical grainsize at which the density stabilizes in the fine range can be roughly constrained knowing the size of the minimum vesicle diameter in the samples (Manville et al. 2002).

The empirical sigmoidal law inferred from Tungurahua's scoria fall layer offers a promising way to obtain high-resolution mass budgets for the whole August 2006 deposit and to improve magnitude-intensity determinations of the event. It may also prove useful when revisiting mass estimates of previous tephra studies (e.g. Taddeucci et al. 2002; Andronico et al. 2009; Araña-Salinas et al. 2010) and improving mass budget calculations from Doppler radar signals (Gouhier and Donnadieu 2008; Valade and Donnadieu 2011).

Conclusion

High-resolution density and componentry analyses in the scoria fall deposit from the August 2006 eruption of Tungurahua volcano, Ecuador, reveals sigmoidal dependence of particle density against grainsize. This pattern essentially reflects vesicularity distribution in porous clast subpopulations, and can be used to determine the mass componentry distributions at all sampling sites. These findings obtained at Tungurahua suggest that the sigmoidal law is applicable to other scoria, and possibly pumice fall layer of basaltic and andesitic compositions. In summary, this study offers a potentially widely applicable new expression to more accurately evaluate the mass of pyroclastic fall deposits and the size of explosive eruptions, and to improve numerical models of tephra dispersal pattern.

Acknowledgements This work is part of a PhD project by J Eychenne and has been completed in the context of a project entitled "Volcanic hazards associated with open-system activity" (Action Incitative of IRD). L Gailler and A Delcamp carried out a great part of the tedious grain counting and pycnometry analysis, and are warmly acknowledged. The authors thank C Bonadonna and J-C Komorowski for comments on an earlier version of the manuscript. Reviews of the manuscript by V Manville and A Durant and editorial handling by J White are warmly acknowledged. This is Laboratory of Excellence ClerVolc contribution no. 32.

References

- Alfano F, Bonadonna C, Delmelle P, Costantini L (2011) Insights on settling velocity from morphological observations. *J Volcanol Geotherm Res* 208:86–98. doi:10.1016/j.jvolgeores.2011.09.013
- Andronico D, Scollo S, Cristaldi A, Ferrari F (2009) Monitoring ash emission episodes at Mt Etna: The 16 November 2006 case study. *J Volcanol Geotherm Res* 180:123–134. doi:10.1016/j.jvolgeores.2008.10.019
- Araña-Salinas L, Siebe C, Macías JL (2010) Dynamics of the ca. 4965yr 14C BP "Ochre Pumice" Plinian eruption of Popocatépetl volcano, México. *J Volcanol Geotherm Res* 192:212–231. doi:10.1016/j.jvolgeores.2010.02.022
- Arrighi S, Principe C, Rosi M (2001) Violent Strombolian and sub-Plinian eruptions at Vesuvius during post-1631 activity. *Bull Volcanol* 63:126–150
- Barsotti S, Neri A (2008) The VOL-CALPUFF model for atmospheric ash dispersal: 2. Application to the weak Mount Etna plume of July 2001. *J Geophys Res* 113:B03209. doi:10.1029/2006JB004624
- Bonadonna C, Phillips JC (2003) Sedimentation from strong volcanic plumes. *J Geophys Res* 108:B72340. doi:10.1029/2002JB002034
- Clark SP (1966) Handbook of physical constants. Geological society of America, inc., New-York, 587 pp
- Costa A, Macedonio G, Folch A (2006) A three-dimensional Eulerian model for transport and deposition of volcanic ashes. *Earth Planet Sci Lett* 241:634–647. doi:10.1016/j.epsl.2005.11.019
- Eychenne J, Le Pennec JL, Troncoso L, Gouhier M, Nedelec JM (2012) Causes and consequences of bimodal grainsize distribution of tephra fall deposited during the August 2006 Tungurahua eruption (Ecuador). *Bull Volcanol* 74:187–205. doi:10.1007/s00445-011-0517-5
- Folch A, Cavazzoni C, Costa A, Macedonio G (2008) An automatic procedure to forecast tephra fallout. *J Volcanol Geotherm Res* 177:767–777. doi:10.1016/j.jvolgeores.2008.01.046
- Gouhier M, Donnadieu F (2008) Mass estimations of ejecta from Strombolian explosions by inversion of Doppler radar measurements. *J Geophys Res* 113:B10202. doi:10.1029/2007JB005383
- Heiken G, Wohletz K (1985) Volcanic Ash. University of California Press, 246 pp.
- Kelfoun K, Samaniego P, Palacios P, Barba D (2009) Testing the suitability of frictional behaviour for pyroclastic flow simulation by comparison with a well-constrained eruption at Tungurahua volcano (Ecuador). *Bull Volcanol* 71:1057–1075
- Le Pennec JL, Ruiz AG, Ramon P, Palacios E, Mothes P, Yepes H (2012) Impact of tephra falls on Andean communities: The influences of eruption size and weather conditions during the 1999–2001 activity of Tungurahua volcano, Ecuador. *J Volcanol Geotherm Res* 217–218:91–103. doi:10.1016/j.jvolgeores.2011.06.011
- Manville V, Segschneider B, White JDL (2002) Hydrodynamic behaviour of Taupo 1800a pumice: implications for the sedimentology of remobilised pyroclastic deposits. *Sedimentology* 49:955–976
- Pioli L, Erlund E, Johnson E, Cashman KV, Wallace P, Rosi M, Granados HD (2008) Explosive dynamics of violent Strombolian eruptions: the eruption of Paricutin Volcano 1943–1952 (Mexico). *Earth Planet Sci Lett* 271:359–368
- Pyle DM (2000) Sizes of volcanic eruptions. In: Sigurdsson H (ed) Encyclopedia of Volcanoes. Academic, pp 263–269
- Samaniego P, Le Pennec JL, Robin C, Hidalgo S (2011) Petrological analysis of the pre-eruptive magmatic process prior to the 2006 explosive eruptions at Tungurahua. *J Volcanol Geotherm Res* 199:69–84. doi:10.1016/j.jvolgeores.2010.10.010
- Scollo S, Del Carlo P, Coltell M (2007) Tephra fallout of 2001 Etna flank eruption: analysis of the deposit and plume dispersion. *J Volcanol Geotherm Res* 160:147–164. doi:10.1016/j.jvolgeores.2006.09.007
- Taddeucci J, Pompilio M, Scarlato P (2002) Monitoring the explosive activity of the July–August 2001 eruption of Mt. Etna (Italy) by ash characterization. *Geophys Res Lett* 29:1230. doi:10.1029/2001GL014372
- Valade S, Donnadieu F (2011) Ballistics and ash plumes discriminated by Doppler radar. *Geophys Res Lett* 38:L22301. doi:10.1029/2011GL049415